Simulation of Rotating Stall in a Whole Stage of an Axial Compressor

Nicolas Gourdain[1]
CERFACS, Toulouse, 31057, France

Stéphane Burguburu[2]
ONERA, Châtillon, 92322, France

Francis Leboeuf[3]
University of Lyon, Ecole Centrale de Lyon, Ecully, 69134, France

Guy Jean Michon[4]
Jean Le Rond d'Alembert Institute, Paris, 75013, France

Aerodynamic instabilities that naturally occur in compression systems, such as surge and rotating stall, largely reduce the life duration and performance of system components. The prediction of the compressor operating range is thus a key parameter for the design of gas turbines. This paper investigates the ability of an unsteady flow solver to simulate the rotating stall phenomenon in the full annulus of an axial compressor stage. A comparison with experimental data indicates that the simulation correctly estimates the stability limit. However the rotating stall flow patterns are different. While measurements show only one full span rotating stall cell (40 Hz), the simulation shows first a part span stall with 10 cells (790 Hz) that evolves then towards a full span stall with 3 cells (170 Hz). A spectral analysis based on numerical results underlines the role of rotor-stator interactions in the development of rotating stall. The effects of downstream volumes and inlet distortions are also discussed, showing the necessity to consider the whole geometry to correctly predict the rotating stall frequency.

Nomenclature

Latin letters

B   =   B-parameter, as defined in Moore and greitzer[5] (-)

C   =   number of rotating stall cells (-)

f   =   frequency (Hz)

h   =   radial position (m)

H   =   compressor span (m)

He   =   helicity ($m^2.s^{-2}$)

k   =   throttle parameter (-)

L_R =   rotor blade chord (m)

---

[1] Doctor, Computational Fluid Dynamics Team
[2] Research Engineer, Applied Aerodynamics Department
[3] Professor, Laboratoire de Mécanique des Fluides et d'Acoustique Ecole Centrale de Lyon, UMR CNRS 5509
[4] Research Engineer, Institut Jean le Rond d'Alembert, University Pierre et Marie Curie

m	=	spatial interaction mode (-)
$N_{R,S}$	=	number of blades (R: rotor, S: stator) (-)
Pi	=	total pressure (Pa)
Ps	=	static pressure (Pa)
Q	=	mass flow ($kg.s^{-1}$)
Q_n	=	nominal mass flow (10.5 $kg.s^{-1}$)
r	=	radius (m)
R	=	gas constant (c_p-c_v=287.058 $J.K^{-1}$)
R_k, S_k	=	modal representation of a blade row defined by Eq. 8 (-)
t	=	time (s)
T	=	rotor passing period ($=2\pi/\Omega_{rotor}$) (s)
Ti	=	total temperature (K)
U_t	=	friction velocity ($m.s^{-1}$)
$V_{x,\theta,z}$	=	normalized absolute velocity components ($V_i/[\gamma RT_{i0}]^{1/2}$) ($m.s^{-1}$)
w	=	Hamming's function defined by Eq. 14
$W_{x,\theta,z}$	=	normalized relative velocity components ($W_i/[\gamma RT_{i0}]^{1/2}$) ($m.s^{-1}$)
y^+	=	non dimensional distance to the wall ($=yU_\tau/\nu$) (-)

Greek letters

θ	=	azimuth (^{o})
γ	=	gas constant (c_p/c_v =1.4) (-)
λ	=	wavelength (m)
ρ	=	density ($kg.m^{-3}$)
Ω	=	rotation speed ($rad.s^{-1}$)
ν	=	kinematic viscosity ($m^2.s^{-1}$)

Subscript / superscript

BPF	=	blade passing frequency

in   =   compressor inlet

out   =   compressor outlet

I.   Introduction

A ERODYNAMIC instabilities are one of the most important issues for compressor designers. Many experimental works (Emmons[1], Day[2]) have already studied these instabilities that occur around the maximum of the total-to-total pressure ratio. However, the basic mechanisms of these flow phenomena are not yet fully understood. Usually the first instability encountered in most compressors is rotating stall that is characterized by one or more cells of stalled flow that rotate at a fraction of the rotor speed. This instability is usually responsible for a performance reduction (efficiency, pressure ratio, etc.) and large vibrations that reduce the blade life duration. Moreover, it can induce surge, a low frequency instability that leads to a mechanical failure of the whole system.

In order to avoid such instabilities, designers usually apply a safety margin called the "surge margin". Unfortunately, this strong constraint limits the efficiency and leads to an over-dimensioning of the compression system. The possibility to reduce the surge margin is thus of a great interest for designers. However, operation closer to the stability limit increases the probability of stall inception. Therefore, it is reliable to reduce the surge margin only if precursors can be detected before instabilities occur (Garnier[3]) and an appropriate action is taken to avoid stall (Dhingra[4]). In the same way, designers are looking for shifting the stability limit towards lower mass flow. It requires a good understanding of the physical mechanisms that are responsible for stall inception and the capacity to control the flow, for example with casing treatments.

The prediction of the stability limit is thus very useful to design high-efficiency compressors that can help improve the gas turbine system in terms of weight, fuel burn and pollutant emissions. Analytical models (Moore[5]) can offer valuable information about the pressure ratio or mass flow rate evolution during rotating stall or surge but do not accurately estimate the stability limit. Moreover, some flow phenomena such as separation in the intake are responsible for inlet distortions that can modify the surge line position (Colin[6]). In that context, one way to improve the prediction of the stall inception point is the use of CFD (Computational Fluid Dynamics). Previous studies show that this approach is able to simulate aerodynamic instabilities (Niazi[7]), even by means of simple methods such as a 2D Euler flow solver (Schmidtmann[8]) or a quasi-3D Navier-Stokes flow solver (Gourdain[9]). Other numerical studies were carried out in order to explore the role of different elements to explain the loss of stability. For example,

Bergner[10] and Inoue[11] point out the role of the tip leakage flow on the stall inception and He[12] shows that rotor-stator interactions can modify the stability limit and the rotating stall configuration.

In that context this work focuses on two aspects: the simulation of rotating stall with a 3D flow solver and the improvement of knowledge about this instability. A difficulty is that no assumption can be done on the spatial periodicity to obtain a correct description of this phenomenon. Following the strategy proposed in previous studies (Sheng[13], Chen[14]), a flow simulation on the entire annulus of the compressor stage is thus necessary. A sufficient physical time should be described to observe the complete development of the rotating stall phenomenon (including transient). The paper is organized as follow. First, the compressor test case is presented, followed by the description of the numerical method, the compressor model and the boundary conditions. The results from the numerical simulations are then compared with experimental data with a particular attention on the rotating stall configuration. A discussion is also proposed to point out the role of inlet distortions and downstream volumes. Finally, the numerical results are analyzed by means of spectral representations. The investigations mainly focus on the role of the tip leakage flow and rotor-stator interactions. A simple extension of the Tyler and Sofrin[15] model is used to complete this analysis.

II. Description of the compressor

The test case considered for this study is the "Cme2" compressor (Faure[16], Fig. 1). This axial subsonic compressor designed by SNECMA is located at the LEMFI laboratory (Orsay, France). It is composed of a single-stage with one rotor of 30 blades and one stator of 40 blades. Table 1 gives some information about the aerodynamic performance and the main geometric parameters. The measured nominal rotation speed is 6330±14 rpm, which corresponds to a relative Mach number at tip of 0.534, thus the flow is perfectly subsonic in the entire compressor. The tip clearance is 0.8% of the rotor span (*i.e.* 0.6% of the rotor blade chord). At the nominal operating point, the mass flow is 10.5±0.1 kg.s^{-1} and the total-to-total pressure ratio is 1.152. At design conditions the value of the B-parameter proposed by Moore and Greitzer[5] is below 1. This parameter is a function of the ratio between the air volumes downstream of the compressor and inside the compressor. Since the B-parameter is small, the probability for this compressor to exhibit a surge phenomenon (and thus the risk of mechanical failure) is low. Experimental investigations at design, off-design and during rotating stall were carried out at the LEMFI laboratory (Michon[17]).
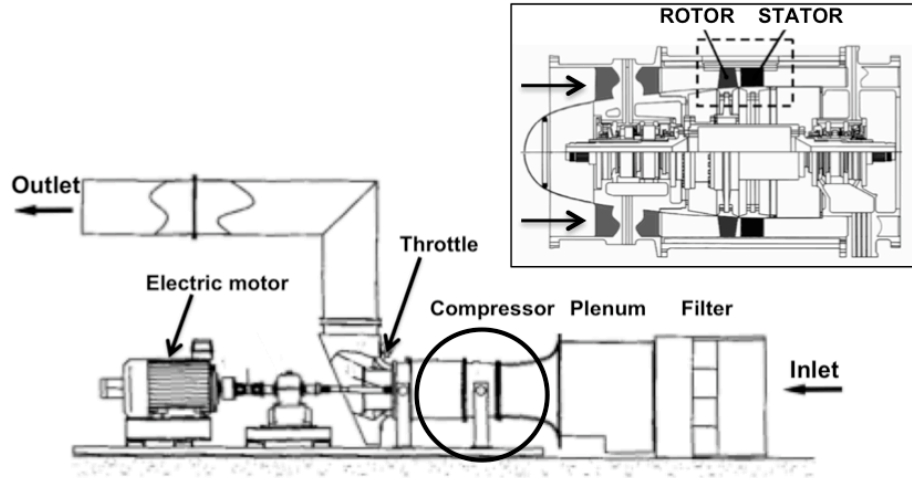
Fig. 1 View of the Cme2 compressor (up) and the experimental facility (down)

Table 1. Compressor description

Nominal pressure ratio	1.152
Nominal mass flow	10.50 kg.s^{-1}
Measured efficiency	0.92
Nominal rotation speed	6330 rpm
Blade Passing Frequency	3165 Hz
Rotor speed at tip	182.0 m.s^{-1}
Shaft power	180 kW
Tip radius	0.275 m
Number of rotor blades	30
Number of stator blades	40
Rotor blade chord	84 mm
Stator blade chord	77 mm
Tip clearance	0.5 mm
Hub to tip ratio	0.78

III. Numerical simulation

A. Flow solver and numerical parameters

Since the simulation of rotating stall requires a time-accurate method, the flow is simulated by solving the unsteady Reynolds-Averaged Navier-Stokes equations (URANS) that describe the conservation of mass, momentum and energy of a viscous fluid. This system of equations is solved with the code "*elsA*" jointly developed by ONERA and CERFACS (Cambier[18]). The partial differential equations are integrated with a compressible Finite Volume formulation method on structured meshes in the reference frame of each row. For this application, convective fluxes

are computed with a 2nd order centered scheme with artificial scalar dissipation (Jameson[19]) and diffusive terms are estimated with a second order centered scheme. The system of equations is closed with the one-equation Spalart-Allmaras turbulence model (Spalart[20]) that represents a good balance between cost and precision. Based on the rotor blade chord, the value of the Reynolds number is estimated to $Re=5.0\times10^5$. As a consequence the flow is assumed to be fully turbulent. To reduce the memory cost, an explicit four stage Runge Kutta scheme is used for time integration (explicit schemes are less memory consuming compared to fully implicit algorithms). To relax the numerical stability constraints, the Runge-Kutta scheme is coupled with an Implicit Residual Smoothing algorithm (Lerat[21]) that allows to reach higher CFL numbers (gain is one magnitude order). This method is second order time accurate. These numerical choices are validated in a preliminary study considering a 3D simplified configuration (Gourdain[9]). This work shows that such an unsteady flow simulation is stable at near stall conditions until a CFL number equal to 20.

Another difficulty is related to the fact that the typical mesh requirements for correct boundary layer resolutions are very restrictive regarding the studied phenomena (instabilities are usually associated with low frequencies with respect to the blade passing frequency that need a long physical time to develop). Two approaches can be applied: either a low-Reynolds method which requires at least 30 points in the boundary layer in the wall-normal direction or a wall-function method that needs less mesh points, allowing larger physical time steps. Despite the fact that the use of a wall function can be critical to compute flow separations, the priority has been given to this approach in order to limit the number of time steps necessary to describe a compressor rotation. The minimum cell size is thus set to 40μm (corresponding to a mean normalized wall distance y^+ of 20). This mesh is thus well adapted for attached flows but results for stalled flows should be interpreted with caution. At the nominal speed (6,330 rpm), one compressor rotation is described with only 10,000 time steps (*i.e.* 10,000/30 time steps by rotor passage). The number of rotations required to obtain a periodic state depends on the operating point. One compressor rotation is enough at nominal operating conditions, but until five rotations are necessary close to the stall inception point. The mass flow history related to a near stall operating point is shown in Fig. 2, indicating that a periodic state is performed only after three rotations of the compressor.
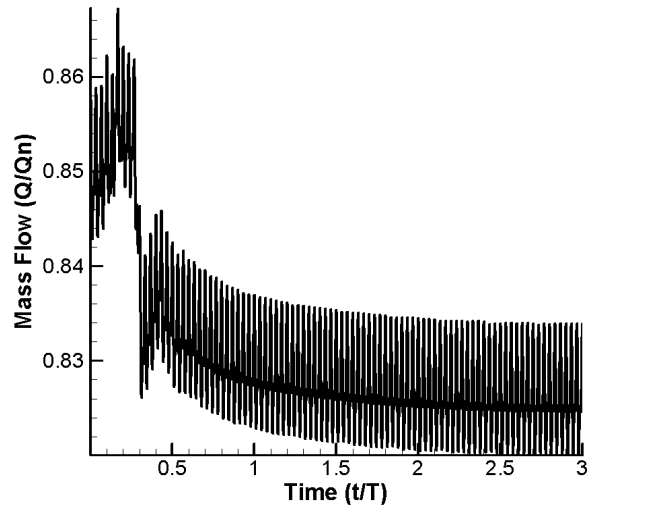
Fig. 2 Evolution of the outlet mass flow at near stall conditions (Q/Q$_n$=0.827)

B. Meshing strategy and boundary conditions

The meshing strategy is based on a multi-block topology (Fig. 3). Each passage is divided into H-grids with one

O-grid around the blade. The tip clearance is taken into account thanks to a single H-type mesh with 11 points in the

radial direction. In order to allow more flexibility on the mesh design, a boundary condition with non-matching

points is used at the interface between the O-grid of the blade and the H-mesh of the tip clearance (grid density is

similar on both sides of the non-matching condition). The number of mesh points is about 500,000 for one rotor

passage and 400,000 for one stator passage. The node distribution in a typical passage is described in table 2. In

order to avoid numerical difficulties like mass flow distortion on the inlet boundary condition, the mesh extends up

to 2 rotor blade chords upstream the rotor leading edge and 2 stator blade chords downstream the stator trailing

edge. At the inlet, the boundary condition is a purely axial injection condition with uniform stagnation pressure and

temperature (boundary layer are not taken into account). Classical downstream boundary conditions (such as a

uniform static pressure) are not sufficient to simulate an operating point near the maximum of pressure ratio. When

the slope of the characteristic becomes null, the calculation cannot perform the fixed downstream pressure and

convergence can become difficult to achieve. A solution is to use a boundary condition with a higher number of

freedom degrees, such as an idealized throttle condition that represents better the experimental facility behavior. A

quadratic law is thus applied at the outlet to determine the static pressure Ps$_{out}$

$$Ps_{out}(t) = Pi_{in} + k.Q(t)^2. \tag{1}$$

The mass flow used to fix the static pressure value corresponds to the instantaneous mass flow computed at the outlet position. A radial equilibrium condition is then applied to compute a static pressure along the compressor span

$$\frac{\partial Ps}{\partial r} = \rho \frac{V_\theta^2}{r}.$$
(2)

The main advantage of this method lies in its ability to capture the outlet static pressure transient and avoid numerical instabilities when the mass flow is reduced. Indeed it has a better capacity to capture physical flow features when instabilities such as rotating stall are studied. A 1D non-reflective condition is associated with the inlet and outlet boundary conditions. With this numerical model, all the operating points of the compressor characteristic can be simulated (including the maximum of pressure ratio): the position of the operating point is set only by means of the throttle parameter k.

Table 2 Node distribution in one passage

(streamwise × pitchwise × spanwise)

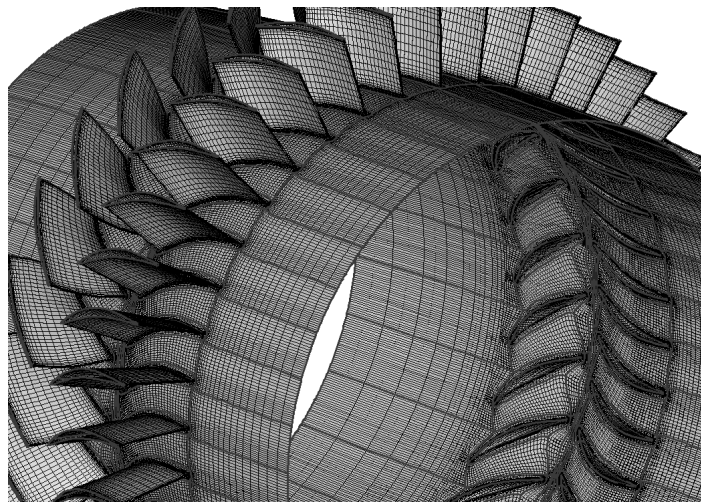|	Rotor	Stator
O-blade	183×19×67	171×19×57
H-upstream	33×57×67	9×47×57
H-channel	59×21×67	67×25×57
H-downstream	15×51×67	39×41×57
H-tip clearance	93×7×11	-
Total	500.415	395.922

Fig. 3 Partial view of the 3D mesh (1 grid point out of 2 is shown)

C. Simulation of the whole stage

No assumption can be done about the flow periodicity necessary to obtain a correct description of rotating stall. However, CPU time constraints do not allow simulating the complete experimental facility. Indeed, while it has been chosen to represent the entire compressor annulus (no assumption is done about azimuthal disturbances), only sections of the inlet and outlet ducts are considered. Upstream and downstream volumes are thus reduced. The mesh described in table 2 is replicated around the annulus in order to simulate the flow in all rotor and stator passages. This approach leads to a mesh of 31 million grid points. One compressor rotation requires 280 CPU hours with four vector processors (NEC-SX6) and the RAM memory consumption reaches 30 GB. Table 3 shows that the mean efficiency of the parallel computation is close to 75% for this application.

Table 3 Performance of the parallel computation

Number of processors	CPU time (µs/iteration/point)	Mflops by processor	Speed-up
1	2.14	2194	1.00
4	0.72	1630	2.97

In order to initialize the full stage simulation, an unsteady flow simulation has been performed at near stall conditions ($Q/Q_n=0.827$), considering only an azimuthal periodic sector of the compressor (three rotor passages and four stator passages). The instantaneous flow field is replicated to obtain the flow in the entire compressor and the throttle parameter k is increased to reach an operating point slightly beyond the stability limit. The full transient from near stall operating conditions to stalled conditions needs 4,000 CPU hours to be obtained.

IV. Comparison with the experimental data

A. Analysis of the results

The experimental measurements reported in this study were obtained with hot wire/cross-film probes. The cross-film probe is intrusive and limited to non-bladed regions (in the present case). The calculation of velocity components (V_x and V_θ) assumes that the velocity vector is orthogonal to the probe axis. While this assumption is roughly true at rotor-stator interface during stable operating conditions, it leads to important uncertainties during rotating stall and the results obtained at stalled conditions have mainly a qualitative interest. The maximum

frequency that can be considered with the two-wire probes is 5,000 Hz (the blade passing frequency is 3,165Hz). More information about measurements and experimental results during rotating stall can be found in Ouayahya[22].

A difficulty lies in the estimation of the stall inception point. While it is experimentally feasible with a reasonable uncertainty ($\Delta Q/Q_n<1\%$), the numerical approach is much more problematic. Steady flow methods using a mixing plane approach are known to be inaccurate at off-design conditions and unsteady flow simulations are very costly when considering the whole periodicity. The solution used in this study is to consider only the spatial periodicity of the compressor that contains all the information related to rotor-stator interactions (*i.e.* 1/10 of the full-annulus in this case). The unsteady flow simulation is then run for 5 compressor rotations on this reduced geometry (less than 4 millions points). An axial velocity signal is registered at the outlet near the casing (at h/H=80%) and a Fourier transform is performed to show the frequencies contained in the signal. When instabilities develop, the Fourier analysis shows that low frequencies appear in the flow. Indeed, the operating point is assumed to be stable if only multiples of the blades passing frequency (BPF) are observed at the end of the simulation.

The numerical compressor characteristic is compared with the experimental one in Fig. 4 at the nominal rotation speed (the ratio $\Omega/T^{1/2}$ is constant). The pressure ratio is well estimated by the simulation in terms of shape and value, especially at low mass flow rates around the pressure peak. The stability limit is also correctly predicted by the simulation since the last stable operating point is found at Q/Qn=0.827 and measurements estimate it at Q/Qn=0.816±0.009 (the difference is thus smaller than 1% of the nominal mass flow). One can note that the stall inception point is found at a mass flow lower than the zero-slope peak of the compressor pressure ratio. First signs of stalled flows are observed close to the rotor casing both with measurements (Michon[17], Ouayahya[22]) and simulation, indicating that this compressor is tip critical at this rotating speed.

Numerical and experimental data are now compared beyond the stability limit, in order to assess the capacity of the unsteady flow simulation to reproduce complex flow physics that occur during the stall process. Two aspects are explored: the transient from stable to unstable conditions and the operating conditions during fully developed rotating stall. The time history of axial velocity signals covering 14 compressor rotations is presented in Fig. 5 (simulation) and Fig. 6 (experiments). For the numerical simulation, time count starts when the throttle parameter *k* was fitted to obtain a rotating stall configuration. For experiments, the time starts after the detection of the first rotating stall sign, known in the literature as a "spike". In both cases, the probe is located in the absolute frame of reference, near the casing (h/H=90%) at rotor-stator interface and in the middle of a stator pitch.

Regarding the transient from the last stable operating point to rotating stall, simulation and experiments show a different behavior. The experimental signal indicates a very short transient (one compressor rotation) before the flow exhibits a fully developed rotating stall. No evolution towards surge is observed, even after thousands of rotations. The pressure ratio is reduced from 1.160 (last stable point) to 1.117 (fully developed rotating stall) with no modification of the mean mass flow. The simulation shows a rotating stall phenomenon after one compressor rotation with a large number of part span cells (10). At this operating point, both pressure ratio and mass flow are reduced (respectively from 1.157 to 1.090 and from Q/Q_n=0.79 to Q/Q_n=0.60). This part span stall is observed in the flow during ten rotations of the compressor. However, after a new transient, the flow evolves towards a full span stall configuration with three rotating stall cells. The compressor performance is slightly better during full span stall (pressure ratio is 1.105 and Q/Q_n= 0.66) than during part span stall. During full span stall, the difference between simulation and experiments is 10% for the time-averaged pressure ratio and 20% for the time-averaged mass flow. The temporal fluctuations of the axial velocity component present similar peak-to-peak values both for numerical and experimental results (50% of the mean axial velocity).
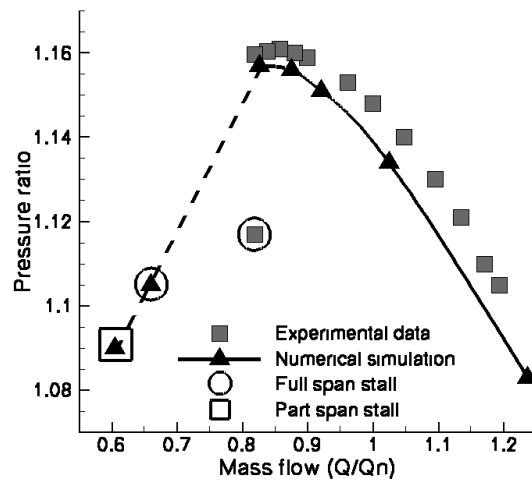

Fig. 4 Pressure ratio with respect to the mass flow

Table 4 summarizes the comparisons between experimental and numerical data regarding the fully established rotating stall configuration. While the determination of the number of cells is straightforward with the numerical simulation, it is more complicated with experiments. To obtain the experimental number of cells, the signals registered by two hot-wire probes located at the same axial position are correlated. This method indicates that only one cell exists in the compressor (Michon[17]) that rotates at 40% of the rotor speed. Figure 7

presents a comparison of the instantaneous axial velocity flow fields upstream the rotor leading edge (x/L_R=-0.11). The experimental field is obtained by phase-averaging the axial velocity component registered by hot cross-film probes (to filter turbulence) and the numerical field is the final instantaneous axial velocity flow field (14th revolution).
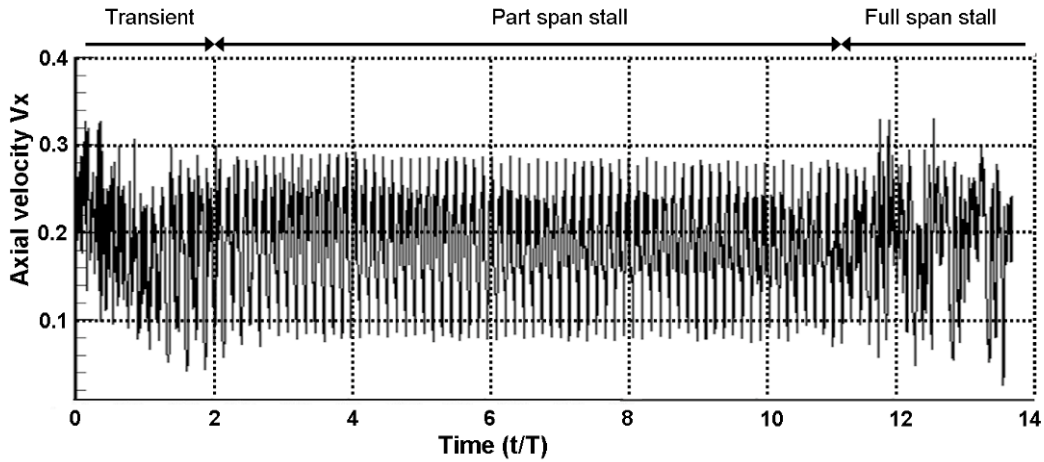

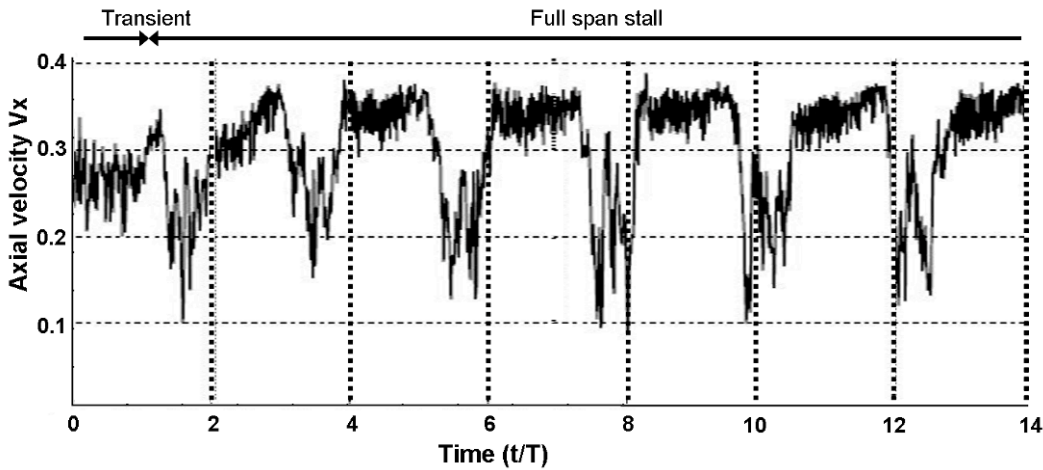**Fig. 5 Normalized axial velocity registered during the numerical simulation (rotor/stator interface, h/H=90%)**

Fig. 6 Normalized axial velocity signal registered by a hot wire probe (rotor/stator interface, h/H=90%)

12
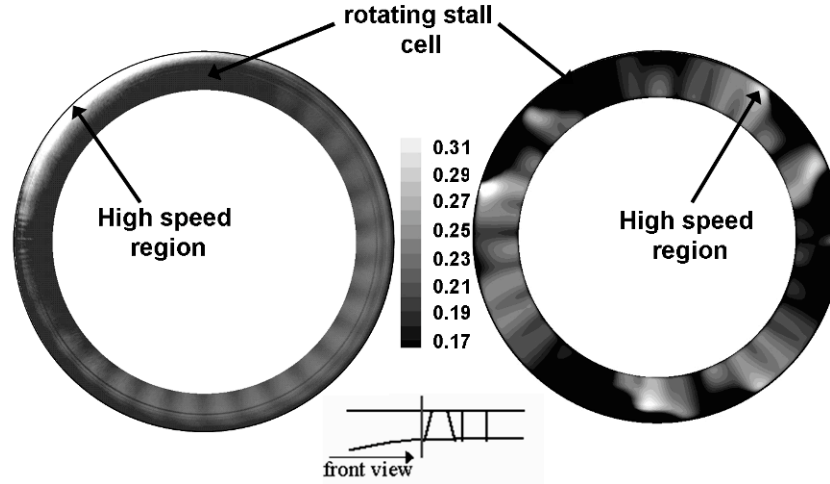
Fig. 7 Comparison of the instantaneous axial velocity flow fields upstream the rotor at x/L$_R$=-0.11, left: hot cross film measurements, right: numerical simulation

The rotating stall cell position is clearly pointed out by the low axial momentum regions. Despite the discrepancy on the number of cells, the circumferential part of the whole compressor annulus that operates at blocked conditions is similar (120° for the experimental results and 144° for the numerical results). As observed in Fig. 7, experiments show a region of high axial velocity inside the cell near the casing, indicating the flow is not fully blocked inside the rotating stall cell. While the simulation also predicts a similar behavior (with a lower intensity), this behavior is not well explained.

Table 4. Final rotating stall characteristics

*(quantities with * are time and mass flow averaged)*

Rotating stall Characteristics	Numerical simulation	Experimental measurements
Stall inception point (Q/Q$_n$)	0.828	0.816±0.009
Number of cells	3 (full span)	1 (full span)
Cell speed (Ω/Ω_{rotor})	0.550	0.400
Flow blockage*	144°	120°
Mass flow* (Q/Q$_n$)	0.724	0.816±0.009
Pressure ratio* (Pi/Pi$_{in}$)	1.105	1.113

B. Discussion

The comparison with experiments indicates that the numerical simulation is not able to predict the number of rotating stall cells. The reasons for such differences with measurements exist and some explanations can be found in

the literature. For example, Spakovszky[23] points out the role of the whole system, including inlet and outlet ducts, in the selection of the most unstable mode (*i.e.* the number of cells in the case of rotating stall) and Day[24] shows the influence of the ratio between the compressor and the downstream volumes on the unstable frequency (*i.e.* the cells rotating speed). In the present case, the simulation does not take into account the presence of four struts upstream of the rotor and the computational domain is shorter than the experimental domain, especially regarding the size of the downstream volume. Therefore it is interesting to investigate the role of two effects in a simplified geometry of the compressor: the downstream duct length and the perturbation of the inlet conditions. Results of this study are partially published in the PhD of Gourdain[25].

To study the role of the duct length, the size of the downstream duct is increased from 2 stator blade chords (initial value) to 6 stator blade chords. This modification increases the value of the B-parameter[5] from 0.25 (initial configuration) to 0.50 (long duct configuration). Figure 8 shows the flow field at stalled conditions colored with static pressure, for the long duct configuration. The rotating stall configuration is composed of one main cell followed by another smaller cell. The frequency of this rotating stall is 36 Hz (close to the experimental value - 40Hz-). A conclusion of this work is that a longer downstream duct leads to a lower unstable frequency (fewer cells moving at a lower rotating speed: $\Omega/\Omega_{rotor}=0.35$ instead of $\Omega/\Omega_{rotor}=0.55$ compared to the initial case). The analytical models of Tauveron[26] and Moore and Greitzer[5] applied to this compressor confirm this result: it shows that large downstream volumes tend to promote instabilities with low frequencies.

The influence of the inlet distortion is studied by adding a simple sinusoidal modulation of the inlet axial velocity (its amplitude corresponds to 50% of the mean axial velocity). Results shown in Fig. 9 indicate the time needed to observe the development of a full span stall configuration, with respect to the wavelength of the inlet perturbation. For example, the introduction of the wavelength $\lambda_{in}=2\pi/4$ mimics the periodicity of the four upstream struts. The final configuration of rotating stall does not depend on the inlet perturbation (same number of cells that move at the same rotating speed). However the time before rotating stall develops is significantly reduced with respect to the non-perturbed case. While about 10 rotations of the compressor are required for the "clean inlet" case, this time is reduced to five rotations for the case $\lambda_{in}=2\pi/4$ and only one rotation for $\lambda_{in}=2\pi$.
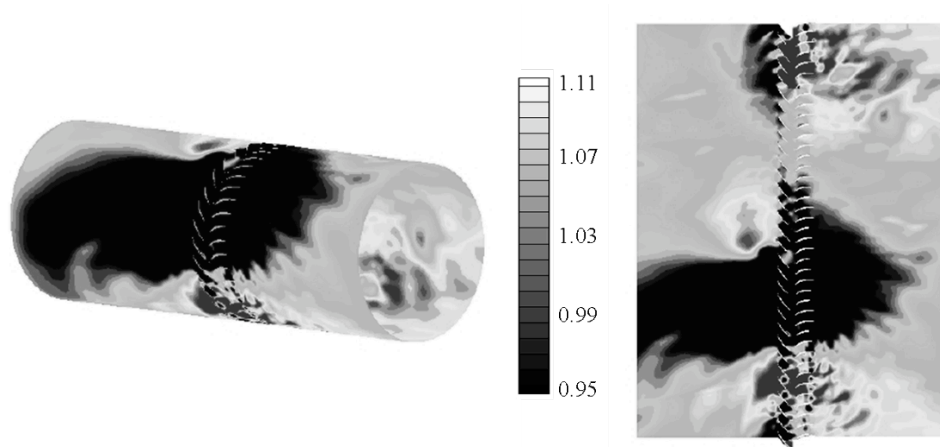
Fig. 8 Instantaneous flow field of static pressure during rotating stall conditions (simulation with long ducts)

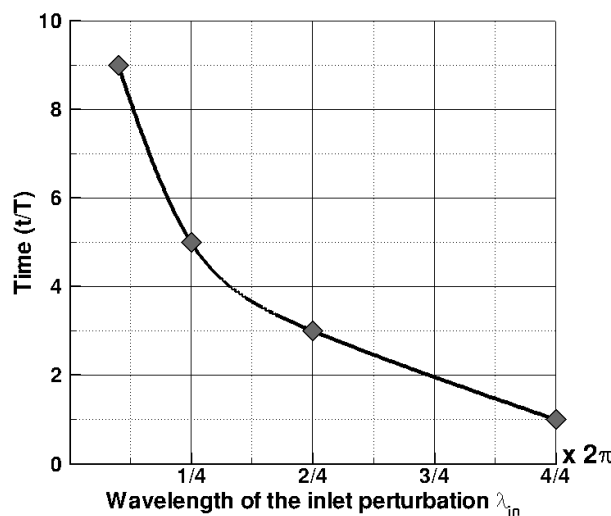
Fig. 9 Time required for the development of rotating stall – influence of the inlet perturbation (the wavelength λ$_{in}$=2π/10 corresponds to a "natural" rotor-stator interaction)

V.   Analysis of the numerical results

A. Development of the rotating stall phenomenon

In the present case, experimental investigations do not provide a sufficient fundamental understanding of the stall inception process and the analysis of numerical results is thus necessary to understand these mechanisms. A spectral decomposition based on discrete Fourier transform of static pressure signals is used to explore the stall development

in the compressor. The signal is registered around the entire compressor annulus at the rotor-stator interface near the casing (h/H=80%). Figure 10 shows the most interesting Fourier modes at different time instant. Each mode is expressed as a fraction of 2π (mode 10 corresponds to the spatial wavelength $2\pi/10$). To complete this analysis, it is necessary to identify the flow frequencies. While a spatial periodicity can always be found, the flow is no longer periodic in time during rotating stall. In consequence, the use of a Fourier transform can lead to high uncertainties. However, it is assumed that a signal covering a sufficient time can reduce this uncertainty. Thus, a Fourier transform is performed considering a static pressure signal during four compressor rotations (from the 8th to the 12th rotation). Results are shown in Fig. 11. Each frequency is normalized with the rotor frequency (105.5 Hz): the mode 30 corresponds thus to the blade passing frequency (3,165 Hz).

  The development of the part span stall (10 cells) is linked to the spatial mode 10. As shown in Fig. 10, this mode grows during the first three compressor rotations before reaching a periodic state with large amplitude fluctuations. This result is correlated with those shown in Fig. 11 to estimate that the 10 cells rotate at 75% of the rotor speed. The part span stall is thus characterized by a frequency of 787 Hz while the frequencies 1574 Hz and 2361Hz can be interpreted as its harmonics. Until the 13th compressor rotation, the mode 10 related to the part span stall has the largest effect on the flow near the casing but has only a small influence below the mid-span (not shown here).
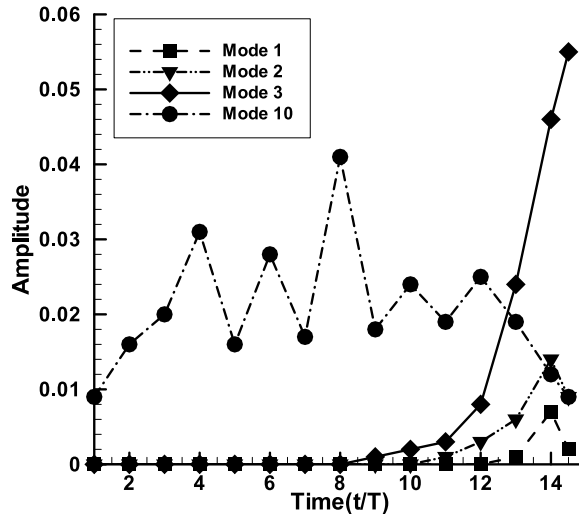

Fig. 10 Evolution of the Fourier spatial modes during the simulation (h/H=80%) – spatial modes are expressed as a fraction of 2π (*i.e. m = $2\pi/\lambda$*)

Figure 10 also indicates that the 3rd spatial mode grows after t/T=9. Contrary to the part span stall, this new spatial mode affects the entire compressor span and becomes the dominant mode in terms of magnitude after the 13th revolution. The result is the development of three full span rotating stall cells and the large reduction of the part span stall influence. The full span stall is characterized by a relatively low frequency (173 Hz) corresponding to three cells moving at 55% of the compressor rotation speed. In the present case, the speed of the stall cells typically decreases with the increased cell size and the number of stall cells typically decreases as the size of the cells increase and coalesce into larger cells. Such a behavior as already been reported during experimental campaigns described in the literature (Day[27]).

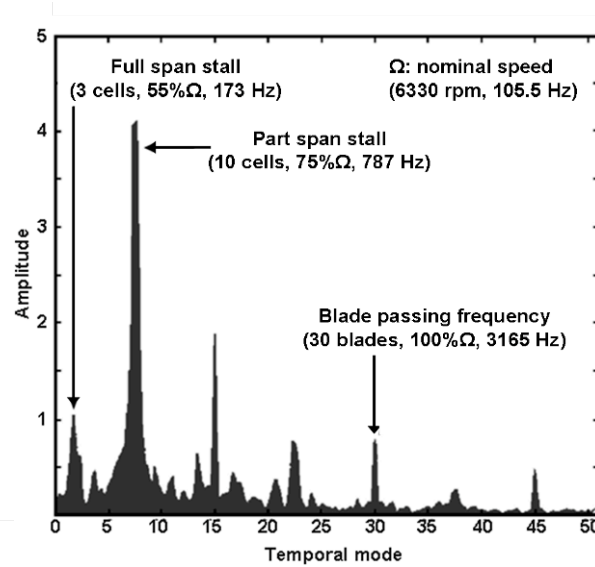**Fig. 11 Fourier transform of a temporal static pressure signal (h/H=80%) – temporal modes are expressed as a multiple of the rotor frequency (105.5 Hz)**

1. Development of the part span stall

The part span stall develops near the rotor casing. This instability is largely driven by the tip leakage flow and the number of cells is clearly related to rotor-stator interactions. The time-averaged flow fields of relative helicity He$_r$ defined as

$$He_r = \vec{W}.rot\,\vec{W} \tag{3}$$

are shown in Fig. 12 and Fig. 13 at two operating points (respectively at near stall conditions and during the transient towards rotating stall). The relative helicity is well suited to track the 3D kinematic effects such as vortices

in the direction of the main flow (while entropy is a good indicator for "past" losses, helicity is more related to potential "future" losses). It is particularly useful in the regions where interactions between two jet flows are observed such as the incoming flow and the tip leakage flow. Figure 12 indicates that two main regions of helicity exist near the casing. The first region is related to a separation of the suction side boundary layer (after 50% of the rotor chord) and the second region is induced by a large vortex that develops near the rotor leading edge. In the present case, the compressor stability is directly linked to the behavior of this Rotor Leading Edge (RLE) vortex. Due to the large momentum of the flow that crosses the tip clearance gap, the vortex crosses the passage and impacts the next rotor blade. At reduced mass flow, the position of the vortex tends to move towards the rotor leading edge (Fig. 13). A flow condition to trigger stall is thus that the tip leakage vortex impacts the leading edge of the next blade. The coupling between the tip leakage vortices leads to a configuration with a ring of blocked flow near the casing, leading to strong shear constraints between the main flow and the blocked flow. This mechanism is very similar to what is reported in the literature by many authors describing such short length-scale disturbances (März[28], Hoying[29,30]). The present study also corroborates the criteria proposed by Vo[31] for the formation of these disturbances (also called "spikes"): the interface between the tip leakage flow and the main flow must be parallel to the rotor leading edges. The present work also takes into account the azimuthal perturbations induced by the stator blades behind the rotor. In this compressor, the Vo's criterion is not obtained simultaneously in all the blade passages and rotor-stator interactions modify the flow angle at the rotor leading edge, meaning the RLE vortex does not impact all the blades at the same axial position. This mechanism is a bit different from the phenomena usually reported in the literature to explain the development of part span stall and it explains why the number of observed part span stall cells is 10 (N_S-N_R=10). However, among a few papers that focus on the flow simulation in a full annulus of a compressor stage (including rotor-stator interactions), some results also indicate that the number of part span stall cells is not always correlated with the blade count (Chen[32]).

In the present case, once the condition for instability is reached in some rotor passages, massive separations occur on the rotor blades and cells develop with a rotating speed lower than the rotor one. The instantaneous entropy flow field shown in Fig. 14 point out the rotating stall cells. In particular the radial and azimuthal extensions of the cells are identified: each cell extends on 50% of the compressor span and two rotor passages. In the present case, the part span stall only affects the flow locally inside the compressor (no global instability is observed).
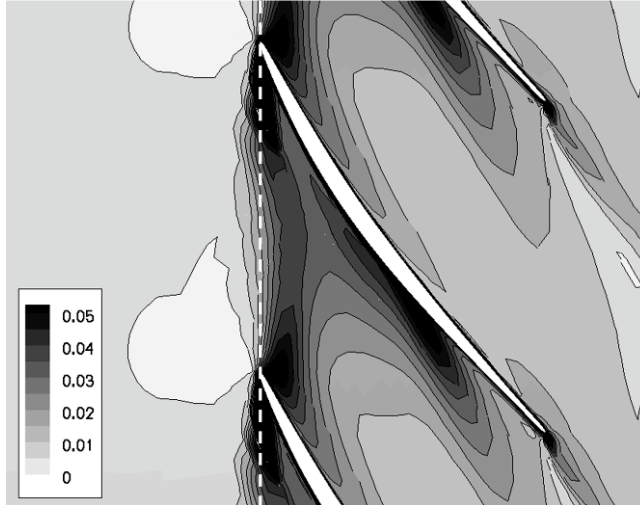
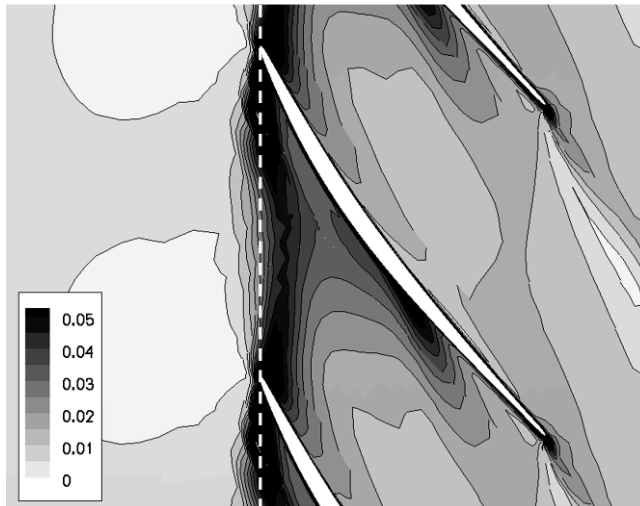**Fig. 12 Time-averaged flow field of relative helicity at near stall conditions (h/H=98%)**

Fig. 13 Time-averaged flow field of relative helicity just before part span stall occurs (h/H=98%)

2. Development of the full span stall

As previously mentioned, the part span stall is not a "stable" configuration and it evolves towards a full span stall phenomenon. Unlike the part span stall, the new number of cells is not driven by rotor-stator interactions. A large wavelength develops behind the part span stall and leads to three full span rotating stall cells that extend on four rotor passages (Fig. 15). During four rotations, both phenomena (part span and full span stalls) are observed simultaneously. However, the part span stall located near the casing is progressively reduced until it completely vanishes. In the present case, the part span stall can thus be interpreted as a precursor of the full span rotating stall. It

is also remarkable that the full span stall cells now clearly extend at least one chord downstream of the compressor, while the part span stall cells were contained into the bladed regions.
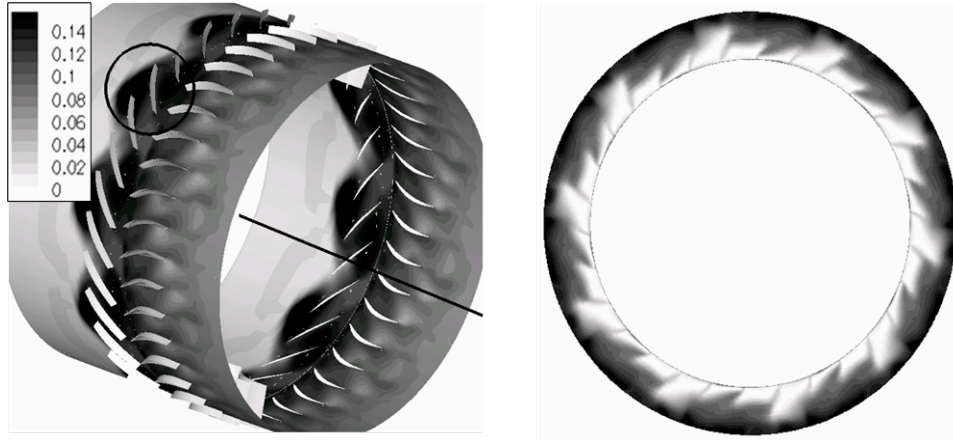

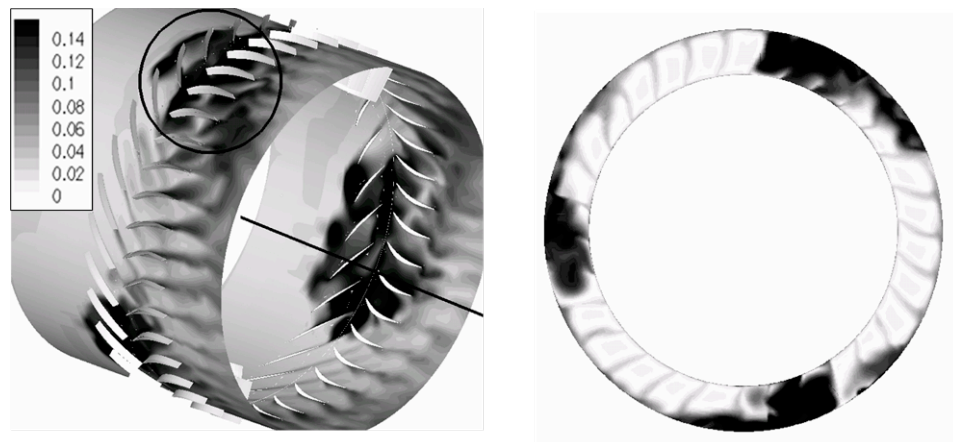**Fig. 14 Instantaneous entropy flow field at t=2T during part span stall (h/H=80% and rotor/stator interface)**

Fig. 15 Instantaneous entropy flow field at t=14T during full span stall (h/H=80% and rotor/stator interface)

B. Theoretical analysis of the cell-blade rows interactions

During rotating stall, the cells interact with the main flow, generating new flow structures. It is assumed that this process is very similar to the interaction between adjacent blade rows. By considering the flow with a modal approach, it is possible to apply a model originally built for rotor-stator interactions to rotating stall. The basic idea is that rotating stall cells behave as a "blade row" with a specific rotating speed and a given number of "blades". The

Tyler and Sofrin[15] (TS) model describes the flow features resulting from the interaction between one rotor and one stator. This model gives the wavelength λ of such flow patterns through the value of their spatial mode m ($=2\pi/\lambda$)

$$m(n,b) = nN_R + bN_S \qquad (4)$$

and their rotation speed Ω_m

$$\Omega_m = \frac{n.N_R}{m}\Omega_R \qquad (5)$$

with n, b: relative integers

Gerolymos[33] has generalized this model to the case considering two contra-rotating rotors. It is thus easy to extend the TS model to the case of a multistage turbomachine, simply by representing each row with a rotating wave that moves in the circumferential direction at a constant speed. The flow distortions seen in the absolute frame and induced by the kth rotor and the kth stator are represented by a simple harmonic wave with a spatial argument ($N_k\theta$) and a time argument ($2\pi ft$). These harmonic waves are given for a rotor by

$$R_k \approx e^{i(2\pi f_k t - a.N_{Rk}\theta)} \qquad (6)$$

and for a stator by

$$S_k \approx e^{i(-b.N_{Sk}\theta)} . \qquad (7)$$

In other words, the flow perturbations induced by the blades are assumed to develop along a straight line in space (t, θ): this is also the basic assumption of the TS model. Interactions between the different blade rows in a multi-stage environment are a combination of the fundamental waves R_k and S_k. In the present case, it is also assumed that each wave can rotate at its own speed Ω_{Rk}. The formalism of the TS model is used to build the Extended Tyler and Sofrin (ETS) model that represents a flow pattern through its spatial mode m

$$m = \sum_k (a_k N_{Rk} + b_k N_{Sk}) \qquad (8)$$

and its rotation speed Ω_m

$$\Omega_m = \frac{\sum_k a_k N_{Rk} \Omega_{Rk}}{m} \tag{9}$$

with k: stage subscript and a_k, b_k: relative integers

One can verify that the result is exactly the TS model if the ETS model is apply to a system composed of one rotor and one stator. Contrary to the TS model, the number of blade rows is no longer limited to two (one rotor and one stator) and a frequency is not necessarily a multiple of the blade passing frequency. These frequencies are easily obtained from Eq. (9) with

$$f_m = \sum_k a_k f_k \tag{10}$$

C. Spectral analysis of the cells-blade rows interactions

Let us now analyze the patterns produced by the interactions between the compressor blade rows and the rotating stall cells. The first difficulty is that the ETS model has a predictive capacity only in the case of a multistage compressor operating at stable conditions. At stalled conditions, the rotating stall configuration has to be known (the values of N_{cells} and Ω_{cells} are *a priori* unknown). The inputs for the ETS model are thus provided by the numerical simulation that shows a full span stall with three cells (Fig. 14) rotating at 55% of the rotor speed Ω (*i.e.* 173 Hz). Indeed, the interest of such a model is to identify the flow patterns that are potentially dangerous for the mechanical integrity of the compressor (blade response due to a forced perturbation). The identification of these flows can also help to detect indirectly surge and rotating stall. Based on Eq. (8) and Eq. (10), a model is built to describe such a three waves system (one rotor row, one stator row and rotating stall cells)

$$m = (a_1 N_R + b_1 N_S) + a_2 C \tag{11}$$

with two fundamental frequencies (related to the rotor and the rotating stall)

$$f_m = a_1 f_{BPF} + a_2 f_{RS} \tag{12}$$

with a_1, a_2, b_1: relative integers, f_{RS}: rotating stall frequency (173 Hz) and f_{BPF}: blade passing frequency (3165 Hz)

In the present case, the studied configuration is N_R=30, N_S=40 and C=3. The flow structures predicted by the model are thus the spatial modes 7, 13, 17, 23, 27, 33, 37, etc. The first predicted frequencies for these flow patterns

are 2992 Hz and 3338 Hz. Obviously, fundamental spatial modes, as modes 3 (cells), 30 (rotor) and 40 (stator), and

fundamental frequencies (173 Hz and 3165 Hz) also exist. To validate these theoretical results, a comparison is done

with a spectral analysis considering the numerical results.

Two kinds of signals are used: spatial signals that are periodic (in the circumferential direction the period is equal

to 2π) and non-periodic temporal signals. For periodic signals, a Fourier transform of a 2D axial velocity signal,

registered at a fixed time (t=14T) and near the casing (h/H=80%), is performed. The vertical axis in Fig. 16 indicates

the value of the spatial Fourier mode *m* while the horizontal axis represents the axial position along the compressor

(inlet is on the left side). Most spatial modes shown in Fig. 16 have only a local effect near the compressor, such as

the modes 7 and 13 which are the results of the interaction between the part span stall (mode 10) and the full span

stall (mode 3). These modes are backward traveling pressure modes as they propagate upstream. A slight influence

for the mode 7 is observed downstream the rotor as a forward traveling pressure wave. However, few modes also

affect the flow far from the compressor. The spatial mode 3 propagates upstream and downstream the compressor

and crosses the boundary of the simulated domain, meaning this mode disturbs and interacts with the entire system.

Remembering that full span rotating stall is an instability that occurs as consequence of a strong interaction between

the compressor and the system, the mode *m*=3 can be seen as a good candidate for the stall inception. Two other

modes have a major effect downstream the compressor: mode 40 related to the stator wakes and mode 37 which is

an interaction between the stator wakes and the full span cells (mode 3). As these modes are mainly entropy modes,
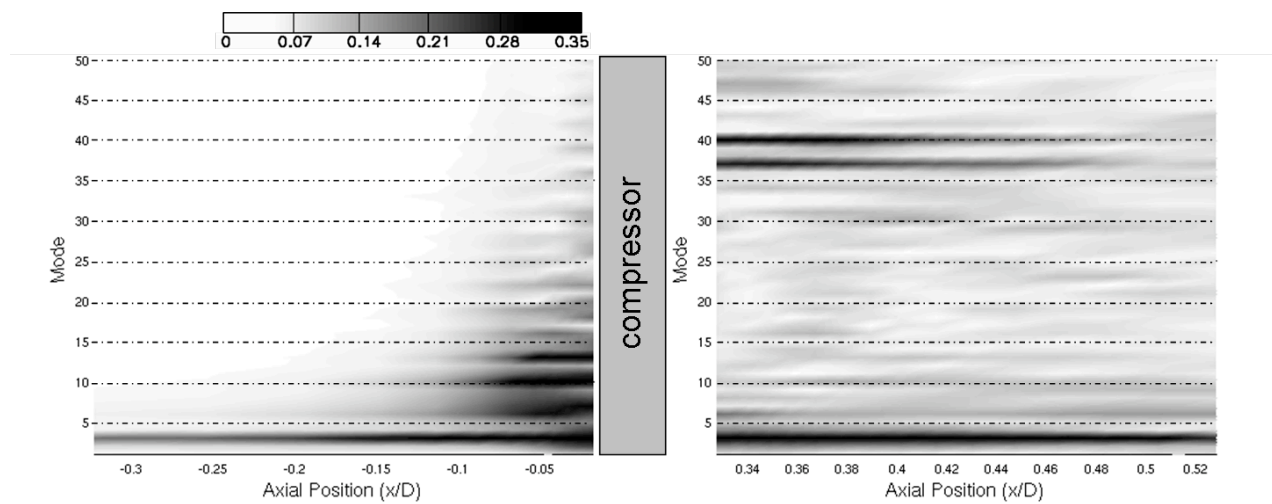
they do not propagate upstream.

**Fig. 16 Spectral power density of the Fourier modes upstream and downstream the compressor
(axial velocity signals, t=14T, h/H=80%)**

Although the influence of the spatial modes has not been estimated *a priori*, the model described by Eq. (11) and Eq. (12) has clearly shown its capacity to estimate the results of the interaction between the rotating stall cells and the blade rows, since all the predicted modes are well observed in Fig. 16.

The second part of the spectral analysis is related to time signals. Due to transient flow and rotating stall, the periodicity for time signals does no longer exist. Thus a simple method to obtain a time-spectral representation of a signal is the Short Time Fourier Transform -STFT- (Allen[34]). The STFT *W* of a signal *s(t)* is computed by

$$W(\lambda, l) = \frac{1}{\sqrt{2\pi}} \int_0^{+\infty} s(t).w(t-l)e^{-i\lambda t} dt$$

(13)

with l, λ: real parameters (time and frequency, respectively).

For this application, the function *w* is the Hamming's function, defined by

$$w(t) = 0.54 - 0.46\cos(\frac{2\pi t}{L})$$

(14)

with L: window length (a low value corresponds to a high resolution in time).

A static pressure signal is registered by a probe located at 80% of the compressor span at the rotor-stator interface and in the middle of a stator pitch. The absolute value of the STFT corresponding to this signal is shown in Fig. 17 with two different window length resolutions. The left side in Fig. 17 corresponds to a "fine" time resolution (the window length is one rotor revolution) while the right side corresponds to a "fine" frequency resolution (the window length is two rotor revolutions). At the end of the second rotor revolution, the dominant frequency is related to the part span stall (787 Hz) and its harmonics. The mode associated to full span rotating stall develops during the 9th revolution (173 Hz) and becomes the most energetic mode after the 13th compressor rotation. Results reported in Fig. 17 (right) indicate that frequencies predicted by the ETS model (2992 Hz and 3338 Hz) are correctly observed. These frequencies are linked to the spatial modes 7 and 13 shown in Fig.16.

This analysis explains partially the flow features during rotating stall. In the present case, the first instability that develops is observed in the tip region (part span stall) and is induced by rotor-stator interactions but at a frequency that is not linked to the rotor speed (*i.e.* the cells speed is not predicted by the TS and ETS models). This particular

rotating stall has only a local influence around the blade rows while the second instability (the full span stall) is more global. While no definitive answer can be proposed to explain the number of full span stall cells, the present analysis strongly suggests that the configuration is induced by the entire system response, as its related spatial mode is observed far upstream and downstream the compressor. Similar observations are also reported in the literature and a few published works indicate that rotating stall can be triggered by a large wavelength flow disturbance (Chen[14]).
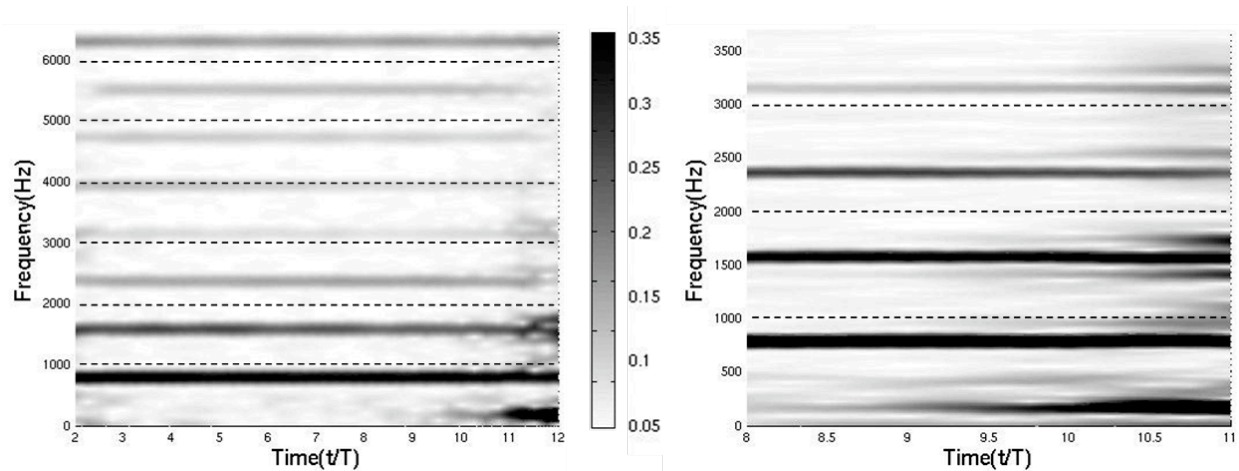

Fig. 17 STFT of a static pressure signal (rotor/stator interface, h/H=80%), left: L=1T (better time resolution), right: L=2T (better frequency resolution)

VI.Conclusion

A 3D unsteady RANS method has been used to compute the flow in the full annulus of an axial compressor stage with the objective to describe the stall inception process. The following points summarize this study.

1- The comparison with experiments validates the numerical method until the stability limit is reached. The mass flow related to the stall inception point is predicted with an error less than 1%.

2- In this compressor the criterion to observe the development of aerodynamic instabilities is the position of the interface between the main flow and the tip leakage flow that must be parallel to the rotor leading edges (as suggested by Vo[31]). Both measurements and simulation found that this compressor is "tip critical".

3- The numerical simulation clearly demonstrates its ability to describe a rotating stall phenomenon, but the number of cells and their rotating speed are not correctly predicted. A conclusion is that a correct simulation of rotating stall

will probably entail the simulation of the entire system geometry of the tested configuration, including upstream and downstream volumes as suggested in the literature (Spakovszky[23], Day[24]).

4- Experimental data shows that rotating stall develops after a very short transient period (one compressor rotation) while the simulation exhibits a complex process that require more than ten rotations (10 part span cells develop first and then merge into 3 full span cells). This point also raises the problem of experimental conditions that are not sufficiently well known at the rotor inlet to properly define the boundary conditions. Disturbances (such as perturbations generated by the upstream struts or endwall boundary layers) probably reduce the time to develop instabilities. Indeed, a "non-perturbed" simulation should be run during a long time (tenth or hundreds compressor rotations) to observe a fully established rotating stall and the transient process can be different.

5- The predicted rotating stall configuration is similar to what is reported in the literature (Day[27]) that indicates short-length scale disturbances (*i.e.* part span stall) have a local effect while large length-scale disturbances (*i.e.* full span stall) are related to a global response of the system. For this application, the full span stall is more energetic (low-frequency around 170 Hz) than the part span stall (790 Hz) and it affects the flow in the whole computational domain.

6- The rotating stall cells interact with the compressor blade rows with the same process as rotor-stator interactions. Based on this observation, an extension of the Tyler and Sofrin model has been proposed to predict the spatial wavelengths and frequencies that develop in the compressor during rotating stall. This information is useful to estimate the risk of mechanical failure due to blade forced response.

Acknowledgments

References

[1] H. W. Emmons, C. E. Pearson and H. F. Grant, "Compressor Surge and Stall Propagation", Transaction of American Society of Mechanical Engineer, Vol. 79, pp. 455-469, 1955

[2] I. J. Day, "Stall and Surge in Axial Flow Compressor" in book Axial Flow Compressor, Lecture Series at Von Karman Institute for Fluid Dynamics, pp. 1-55, 1992

[3] V. H. Garnier, "Experimental Investigation of Rotating Waves as a Rotating Stall Inception Indication in Compressors", GTL Report #198, Massachusetts Institute of Technology, 1989

[4] M. Dhingra, Y. Liu, Y. Neumeier and J. V. R. Prasad, " Compressor Stability Detection on a Turboshaft Engine with a Hybrid Axi-Centrifugal Compressor", 43rd AIAA Joint Propulsion Conference, paper AIAA 2007-5058, Cincinnati, USA, 2007

[5] F. K. Moore and E. M. Greitzer, "A Theory of Post-Stall Transients in Axial Compression Systems: Part I - Development of Equations, Part II – Applications", American Society of Mechanical Engineer, paper 85-GT-171 and 85-GT-172, 1985

[6] Y. Colin, B. Aupoix, J. F. Boussuge and P. Chanez, "Numerical simulation and analysis of crosswind inlet flows at low Mach numbers", Proceedings of the 8th International Symposium on Experimental and Computational Aerothermodynamics of Internal Flows, Lyon, France, 2007

[7] S. Niazi, "Numerical Simulation of Rotating Stall and Surge Alleviation in Axial Compressor", PhD Dissertation, Georgia Institute of Technology, USA, 2000

[8] O. Schmidtmann and J. M. Anders, "Route to Surge for a Throttled Compressor-A Numerical Study", J. of Fluids and Structures, Vol. 15, pp. 1105-1121, 2001

[9] N. Gourdain, S. Burguburu, F. Leboeuf and H. Miton, "Numerical Simulation of Rotating Stall in a Subsonic Compressor", J. of Aerospace Science and Technology, Vol. 10, pp. 9-18, 2006

[10] J. Bergner, D. K. Hennecke and C. Hah, "Tip Clearance Variations of an Axial High-Speed Single Stage Transonic Compressor", 17th Symposium on Air-Breathing Engines, paper ISABE-2005-1096, Munich, Germany, 2005

[11] M. Inoue, M. Kuroumaru, S. Yoshida, T. Minami, K. Yamada and M. Furukawa, "Effect of Tip Clearance on Stall Evolution Process in a Low-Speed Axial Compressor Stage", ASME Turbo Expo, paper GT2004-53354, 2004

[12] L. He, "Computational Study of Rotating-Stall Inception in Axial Compressors", J. of Propulsion and Power, Vol. 13, 1997

[13] S. Sheng, "Full Annulus Simulations of a High-Speed Centrifugal Compressor Using an Unstructured RANS Flow Solver", ASME Turbo Expo, paper GT2004-53657, Vienna, Austria, 2004

[14] J. P. Chen, M. D. Hathaway and G. P. Herrick, "Pre-Stall Behavior of a Transonic Axial Compressor Stage via Time-Accurate Numerical Simulation", ASME Turbo Expo, paper GT2007-27926, Montreal, Canada, 2007

[15] J. M. Tyler and T. G. Sofrin, "Axial Flow Compressor Noise Studies", Society of Automotive Engineers Transactions, Vol. 70, pp. 309-332, 1962

[16] T. M. Faure, G. J. Michon, H. Miton and N. Vassilieff, "Laser Doppler Anemometry Measurement in an axial compressor stage", J. of Propulsion and Power, Vol. 17, Issue 3, pp. 481-491, 2001

[17] G. J. Michon, H. Miton and N. Ouayahya, "Unsteady Three-Dimensional Off-design Velocity and Reynolds Stresses in an Axial Subsonic Compressor", J. of Propulsion and Power, Vol. 21, Issue 6, pp. 961-972, 2005

[18] L. Cambier and J. P. Veuillot, "Status of the elsA CFD Software for Flow Simulation and Multidisciplinary Applications", 46th AIAA Aerospace Science Meeting and Exhibit, AIAA paper 2008-664, Reno, USA, 2008

[19] A. Jameson, W. Schmidt and E. Turkel, "Numerical Solution of the Euler Equations by Finite Volume Methods using Runge-Kutta Time Stepping Schemes", 14th Fluid and Plasma Dynamics Conference, AIAA paper 81-1259, Palo Alto, USA, 1981

[20] P. R. Spalart and S. R. Allmaras, "A One Equation Turbulence Model for Aerodynamic Flows", 30th Aerospace Science Meeting and Exhibit, AIAA paper 92-0439, Reno, 1992

[21] A. Lerat, J. Sides and V. Daru, "An implicit finite-volume method for solving the Euler equations", 8th International Conference on Numerical Methods in Fluid Dynamics, Vol. 170, pp. 341-349, 1982

[22] N. Ouayahya, "Experimental Analysis of the Rotating Stall Inception in an Axial Compressor", PhD dissertation, Pierre et Marie Curie university, Paris, 2009

[23] Z. Spakovszky, "Application of Axial and Radial Compressor Dynamic System Modeling", PhD dissertation, Massachusetts Institute of Technology, USA, 2001

[24] I. J. Day, "Axial Compressor Performance during Surge", J. of Propulsion and Power, Vol. 10, pp. 329-336, 1994

[25] N. Gourdain, "Numerical Simulation of Rotating Stall Phenomena in Axial Compressors", PhD Dissertation, n° 2005-33, Ecole Centrale de Lyon, France, 2005

[26] N. Tauveron, P. Ferrand, F. Leboeuf, N. Gourdain and S. Burguburu, "A Numerical Contribution to the Analysis of Surge Inception and Development in Axial Compressors", ISUAAAT conference, Moscow, Russia, 2006

[27] I. Day, T. Breuer, J. Escuret, M. Cherrett and A. Wilson, "Stall Inception and the Prospects for Active Control in Four High-Speed Compressors", J. of Turbomachinery, Vol. 121, Issue 1, pp. 18-27, 1999

[28] J. März, C. Hah and W. Neise, "An Experimental and Numerical Investigation into the Mechanisms of Rotating Instability", Transaction of American Society of Mechanical Engineers, Vol. 124, pp. 367-375, 2002

[29] D. A. Hoying, "Blade Passage Flow Structure Effects on Axial Compressor Rotating Stall Inception", PhD Dissertation, Massachusetts Institute of Technology, USA, 1996

[30] D. A. Hoying, C. S. Tan, H. D. Vo and E. M. Greitzer, "Role of Blade Passage Flow Structures in Axial Compressor Rotating Stall Inception", J. of Turbomachinery, Vol. 121, Issue 4, pp. 735-742, 1999

[31] H. D. Vo, C. S. Tan and E. M. Greitzer, "Criteria for Spike Initiated Rotating Stall", J. of Turbomachinery, Vol. 130, Issue 1, 2008

[32] J-P. Chen, R. S. Webster, M. D. Hathaway, G. P. Herrick and G. J. Skoch, "Numerical Simulation of Stall and Stall Control in Axial and Radial Compressors", 44th AIAA Aerospace Sciences Meeting and Exhibit, AIAA-2006-0418, Reno, USA, 2006

[33] G. A .Gerolymos, G. J. Michon and J. Neubauer, "Analysis and Application of Chorochronic Periodicity in Turbomachinery Rotor/Stator Interaction Computations", J. of Propulsion and Power, Vol. 18, pp. 1139-1152, 2002

[34] J. B. Allen and L. R. Rabiner, "A Unified Approach to Short-Time Fourier Transform Analysis and Synthesis", Proceedings of the Institute of Electrical and Electronics Engineers Transaction, Vol. 65, pp.1558-1564, 1977